Crystalline particle packings on a sphere with long-range power-law potentials

Mark J. Bowick,[1] Angelo Cacciuto,[1,2] David R. Nelson,[3] and Alex Travesset[4]

[1]*Physics Department, Syracuse University, Syracuse, New York 13244-1130, USA*
[2]*Department of Materials Science and Engineering, University of Illinois at Urbana-Champaign, Urbana, Illinois 61801, USA*
[3]*Lyman Laboratory of Physics, Harvard University, Cambridge, Massachusetts 02138, USA*
[4]*Physics Department, Iowa State University and Ames Laboratory, Ames, Iowa 50011, USA*

The original Thomson problem of "spherical crystallography" seeks the ground state of electron shells interacting via the Coulomb potential; however one can also study crystalline ground states of particles interacting with other potentials. We focus here on long-range power-law interactions of the form $1/r^\gamma$ ($0 < \gamma < 2$), with the classic Thomson problem given by $\gamma = 1$. At large R/a, where R is the sphere radius and a is the particle spacing, the problem can be reformulated as a continuum elastic model that depends on the Young's modulus of particles packed in the plane and the universal (independent of the pair potential) geometrical interactions between disclination defects. The energy of the continuum model can be expressed as an expansion in powers of the total number of particles, $M \sim (R/a)^2$, with coefficients explicitly related to both geometric and potential-dependent terms. For icosahedral configurations of 12 five-fold disclinations, the first nontrivial coefficient of the expansion agrees with explicit numerical evaluation for discrete particle arrangements to four significant digits; the discrepancy in the fifth digit arises from a contribution to the energy that is sensitive to the particular icosadeltahedral configuration and that is neglected in the continuum calculation. In the limit of a very large number of particles, an instability toward grain boundaries can be understood in terms of a "Debye-Huckel" solution, where dislocations have continuous Burgers' vector "charges." Discrete dislocations in grain boundaries for intermediate particle numbers are discussed as well.

I. INTRODUCTION

The Thomson problem of constructing the ground state of (classical) electrons interacting with a repulsive Coulomb potential on a sphere[1] has a rich, approximately 100 year old history.[2–4] Determining crystalline particle packings in curved geometries has a number of interesting applications in physics, mathematics, chemistry, and biology particularly if one allows more general interactions amongst the particles.

An almost literal realization of the Thomson problem is provided by multielectron bubbles.[5,6] Electrons trapped on the surface of liquid helium by a submerged, positively charged capacitor plate have long been used to investigate two dimensional melting.[7,8] Multielectron bubbles result when a large number of electrons ($10^5 - 10^7$) at the helium interface subduct in response to an increase in the anode potential and coat the inside wall of a helium vapor sphere of radius $10 - 100$ microns. Typical electron spacings, both at the interface and on the sphere, are of order 2000 Ångstroms, so the physics is entirely classical, in contrast to the quantum problem of electron shells which originally motivated Thomson.[1] Information about electron configurations on these bubbles can, in principle, be inferred from studying capillary wave excitations.[9] Similar electron configurations should arise on the surface of liquid metal drops confined in Paul traps.[10]

A Thomson-type problem also arises in determining the arrangements of the protein subunits which comprise the shells of spherical viruses.[11,12] Here, the "particles" are clusters of protein subunits arranged on a shell. Although the proteins interact predominantly with short-range van der Waals potentials, the same issues of spherical crystallography arise in these protein shells as in the original Thomson problem. In spherical viruses, 12 of these protein clusters sit at the vertices of a regular icosahedron in a five-fold symmetric environment. The remaining "particles" have six neighboring clusters. This problem of protein arrangements was solved in a beautiful paper by Caspar and Klug[11] for intermediate values of R/a, where R is the sphere radius and a is the mean particle spacing. Caspar and Klug constructed icosadeltahedral particle packings characterized by integers P and Q, which provide regular tessellations of

$$M = 10(P^2 + PQ + Q^2) + 2, \tag{1}$$

protein clusters, or "particles," on the sphere. Most known viruses (examples with M as large as 1472 are known[13–15]) fall into this classification scheme, and can be studied by use of the continuum methods discussed in this paper.[16] The Caspar-Klug tessellations of the sphere provide an excellent starting point for finding low energy particle configurations on the sphere for intermediate values of $M \approx (8\pi/\sqrt{3}) \times (R/a)^2$. Particles numbers M not in the form of Eq. (1) can be accommodated by introducing vacancies or interstitials into these regular packings (see Ref. 17 for a discussion of vacancy and interstitial energies with power-law potentials in flat space). New ground states involving grain boundaries are needed, however, for $M > M_c \approx 400 - 600$, and in particular in the limit $M \to \infty$.[18–21,57]

Other realizations of Thomson-type problems include regular arrangements of colloidal particles in "colloidosome" cages[22–24] proposed for protection of cells or drug-containing

vesicles[25] and fullerene patterns of carbon atoms on spheres[26] and other geometries. An example with long-range (logarithmic) interactions is provided by the Abrikosov lattice of vortices which would form at low temperatures in a superconducting metal shell with a large monopole at the center.[27] In practice, the "monopole" could be approximated by the tip of a long thin solenoid.

The problem of best possible packing on spheres has also applications in the micropatterning of spherical particles[28] relevant for photonic crystals or Clathrin cages, responsible for the vesicular transport of cargo in cells[29] (see Ref. 30 for a detailed theoretical study). Crystalline domains covering a fraction of the sphere are also of experimental interest. In the context of lipid rafts,[31] confocal fluorescence microscopy studies have revealed the coexistence of fluid and solid domains on giant unilamellar vesicles made of lipid mixtures. The shapes of these solid domains include stripes of different widths and orientations.[32–34] The application of spherical elasticity to predict shapes of lipid mixtures domains has been discussed in Refs. 35 and 36.

In the continuum approach used here, details associated with different particle interactions for the system discussed above are parametrized by a bulk and shear elastic constant and a defect core energy. In practice, defect patterns involving dislocations and disclinations depend only on the Young's modulus and a core energy,[21] which can be determined from flat particle configurations. Although we concentrate on the computationally challenging problem of long-range power-law potentials, explicating and complementing previous results,[37] it would be straightforward to treat short-range potentials as well.[4]

The organization of the paper is as follows. In Sec. II, some known results for crystals on curved surfaces are reviewed and several results are obtained. The free energy of the system is described in Sec. III. The particular case of the sphere, the Thomson problem, is discussed in Sec. IV, and several predictions for spherical lattices with icosahedral symmetry are obtained and compared with the results of direct minimizations of discrete icosadeltahedral particle arrays. The solution of the Thomson problem for a very large number of particles is discussed in Sec. V. Section VI contains a summary and conclusions, and some technical results are discussed in the appendixes.

II. CRYSTALS OF POINT PARTICLES

Consider a collection of classical point particles constrained to a frozen (nondynamical) two-dimensional (2D) surface $\mathcal{K}$ embedded in three-dimensional (3D) Euclidean space. The particles interact through a general potential defined in the three-dimensional embedding space or solely within the 2D curved surface itself. This paper focuses primarily on the potential

$$V(\vec{R}) = \frac{e^2}{|\vec{R}|^\gamma}. \tag{2}$$

Here, e is an "electric charge" such that if R is some quantity with dimensions of length,

e^2/R^γ = dimension of energy.

The case $\gamma=1$ corresponds to the Coulomb potential in three dimensions. Allowing we do not treat this problem explicitly here, the replacement

$$V(\vec{R}) \rightarrow \frac{e^2}{\gamma}(|\vec{R}|^{-\gamma} - 1), \tag{3}$$

allows us to treat the two-dimensional Coulomb potential by taking the limit $\gamma \rightarrow 0$,

$$V(\vec{R}) \rightarrow -e^2 \ln(|\vec{R}|). \tag{4}$$

The electrostatic energy of a system of M particles at positions $\vec{R}(\mathbf{1})$, interacting via Eq. (2), with $\mathbf{1}=(l_1,l_2)$, $l_1,l_2 \in \mathcal{Z}$, becomes

$$2E_0 = \sum_{\mathbf{1} \neq \mathbf{1}'}^{M} \frac{e^2}{|\vec{R}(\mathbf{1}) - \vec{R}(\mathbf{1}')|^\gamma}. \tag{5}$$

Note that with this definition the power law interaction acts across a cord of the sphere, as would be the case for electron bubbles in helium. The focus of this paper is the study of crystals on curved surfaces, in particular spherical crystals. There are, however, some quantities which are insensitive to the curvature of the surface, and the simpler geometry of the plane can be used to compute them. The following two sections hence focus on planar crystalline arrays of particles interacting via the potential Eq. (2).

A. Planar crystals

The electrostatic energy Eq. (5) and the corresponding elastic tensor, from which follows the elastic constants of the system, may be explicitly computed for crystalline orderings of particles in a triangular lattice.

For any noncompact surface $\mathcal{K}$, like the plane, the energy Eq. (5) is divergent for all $\gamma \leq 2$. If $\gamma > 0$, the divergence comes exclusively from the zero mode $\vec{G}=0$ associated with the thermodynamic limit of a infinite system size. This term (which would be subtracted off if a uniform background charge were present) can be isolated by setting $\vec{G} \equiv \varepsilon \ll 1$ for this mode. The detailed calculation is somewhat involved and is given in Appendix A. The final result for the ground state energy reads

$$2E_0 = -\frac{Me^2}{\Gamma(\gamma/2)}\left(\frac{\pi}{A_C}\right)^{\gamma/2}\left(\frac{4}{\gamma(2-\gamma)} - \sigma(\gamma)\right)$$

$$+ Me^2\frac{\pi}{A_C}\frac{\Gamma\left(1-\frac{\gamma}{2}\right)}{\gamma/2}\lim_{\vec{G}\to\varepsilon}\frac{2^{2-\gamma}}{|\vec{G}|^{2-\gamma}}$$

$$\equiv Me^2\theta(\gamma)\left(\frac{4\pi}{A_C}\right)^{\gamma/2} + Me^2\frac{\pi}{A_C}\frac{\Gamma\left(1-\frac{\gamma}{2}\right)}{\gamma/2}\lim_{\vec{G}\to\varepsilon}\frac{2^{2-\gamma}}{|\vec{G}|^{2-\gamma}}. \tag{6}$$

A_C is the area of the unit cell of the triangular Bravais lattice

TABLE I. Coefficients of the response function Eq. (9) and the energy Eq. (6). Results are accurate up to six digits. The coefficient ρ is a rational function of γ.

γ	η	ρ	$-\theta$	γ	η	ρ	$-\theta$
1.875	0.699652	31	47.763	0.875	0.199772	23/9	3.2471
1.75	0.619256	15	22.647	0.75	0.159010	11/5	2.7138
1.625	0.544152	87/9	14.288	0.625	0.122622	21/11	2.283
1.5	0.474268	7	10.118	0.5	0.090439	5/3	1.9294
1.375	0.409548	27/5	7.625	0.375	0.062279	1.46154[a]	1.6352
1.25	0.349812	13/3	5.9701	0.25	0.037955	9/7	1.3881
1.125	0.295033	25/7	4.7955	0.125	0.017265	43/30	1.1787
1	0.245065	3	3.9210				

[a]($\gamma=0.375$) a rational number for ρ accurate to six digits could not be guessed.

$[A_C=(\sqrt{3}/2)a^2]$ and Γ is the Euler gamma function. The coefficient σ is a sum over Misra functions, defined in Eq. (B2) of Appendix B. The coefficient $\theta(\gamma)$ parametrizes the nonsingular part of the energy; its dependence on the exponent γ is shown in Table I. This negative quantity parametrizes the binding energy of the triangular lattice after the positive "zero mode" contribution is subtracted off. For $\gamma=1$, we have a two-dimensional "jellium" model. In the problem considered in the introduction, no neutralizing background is present, and the energy is rendered finite by restricting the crystal to a compact surface, like the sphere. The maximum distance between points in the surface will then provide an infrared cutoff.

For small displacements of the particles from their equilibrium positions, one has

$$E - E_0 = \frac{e^2}{2} \sum_{\mathbf{1} \neq \mathbf{1}'} \left(\frac{1}{|\vec{R}(\mathbf{1}) + \vec{u}(\mathbf{1}) - \vec{R}(\mathbf{1}') - \vec{u}(\mathbf{1}')|^\gamma} \right.$$
$$\left. - \frac{1}{|\vec{R}(\mathbf{1}) - \vec{R}(\mathbf{1}')|^\gamma} \right), \quad (7)$$

where $\vec{u}(\mathbf{1})$ is a small displacement of the particle $\mathbf{1}$ in the plane of the surface from its equilibrium position $\vec{R}(\mathbf{1})$, and therefore a tangent vector to the surface $\mathcal{K}$. The elastic tensor $\Pi_{\alpha,\beta}(\mathbf{1},\mathbf{1}')$ is defined as the leading term in an expansion of Eq. (7),

$$E - E_0 = \frac{e^2}{2} \sum_{\mathbf{1},\mathbf{1}'} \Pi_{\alpha\beta}(\mathbf{1},\mathbf{1}') u_\alpha(\mathbf{1}) u_\beta(\mathbf{1}'). \quad (8)$$

In deriving Eq. (7), we assume a constraint of fixed area per particle, enforced by a uniform background charge density or boundary conditions. This eliminates the term linear in $u_\alpha(\mathbf{1})$. The physical properties of response functions are better studied in Fourier space. The detailed calculation is given in Appendix A. The final result is

$$\Pi_{\alpha\beta}(\vec{p}) = A_C \sum_l e^{i\vec{p}\cdot\vec{R}(\mathbf{1})} \Pi_{\alpha\beta}(\mathbf{1},0)$$
$$= \frac{2^{2-\gamma}\pi}{A_C} \frac{\Gamma(1-\gamma/2)}{\Gamma(\gamma/2)} \frac{p_\alpha p_\beta}{|\vec{p}|^{2-\gamma}} + \frac{\eta(\gamma)}{A_C^{\gamma/2}}$$
$$\times [|\vec{p}|^2 \delta_{\alpha\beta} + \rho(\gamma)(\delta_{\mu\alpha}\delta_{\nu\beta} + \delta_{\mu\beta}\delta_{\nu\alpha})p_\mu p_\nu] + O(|\vec{p}|^4). \quad (9)$$

The coefficients $\eta(\gamma)$ and $\rho(\gamma)$ depend only on the potential. In Table I, some values of the coefficients for a range of potentials with $0 < \gamma < 2$ are listed.

B. Continuum free energy

When the deviations from the ground state are small, the long wavelength lattice deformations may be described by a continuous Landau elastic energy

$$F(u) = \int d^2\mathbf{r} \left(\mu u_{\alpha\beta}^2 + \frac{\lambda}{2} u_{\alpha\alpha}^2 \right). \quad (10)$$

The couplings λ and μ are the usual Lamé coefficients. The strain tensor $u_{\alpha\beta}$ is defined by

$$u_{\alpha\beta} = \frac{1}{2}(\partial_\alpha u_\beta + \partial_\beta u_\alpha), \quad (11)$$

where $\vec{u}(\mathbf{x})$ are the small displacements of Eq. (8). The elastic tensor Eq. (8), within Landau elastic theory, is then

$$e^2 \Pi_{\alpha\beta}(\vec{p}) = A_C[\mu|\vec{p}|^2 \delta_{\alpha\beta} + (\lambda + \mu)p_\alpha p_\beta]. \quad (12)$$

A comparison with Eq. (9) immediately yields an explicit expression for the elastic constants of the crystal

$$\mu = \eta(\gamma)\frac{e^2}{A_C^{1+\gamma/2}}, \quad \lambda = \infty, \quad (13)$$

$$Y = \frac{4\mu(\lambda + \mu)}{2\mu + \lambda} = 4\eta(\gamma)\frac{e^2}{A_C^{1+\gamma/2}}, \quad (14)$$

where Y is Young's modulus. The result $\lambda=\infty$ is equivalent to a divergent compressional sound velocity as $\vec{p}\to 0$ and for $\gamma=1$ is just a statement of the incompressibility of a two-
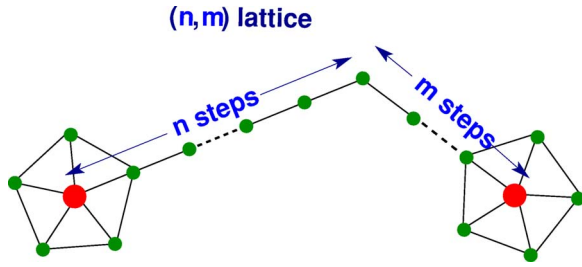
FIG. 1. (Color online) Construction of an (n,m) icosadeltahedral lattice. The filled circles indicate two nearest-neighbor fivefold disclinations. Because these defects sit on the vertices of an icosahedron, they are separated by a geodesic distance $R\cos^{-1}(1/\sqrt{5})$, where R is the sphere radius.

dimensional Wigner crystal. Alternatively, we can allow for wave-vector-dependent elastic constants $\mu(p)$ and $\lambda(p)$ in Eq. (12). In this case $\lambda(p)$ diverges as $p\to 0$,

$$\lambda(p) \approx \frac{2^{2-\gamma}\pi}{A_C}\frac{\Gamma(1-\gamma/2)}{\Gamma(\gamma/2)}\frac{1}{p^{2-\gamma}},$$

while $\lim_{p\to 0}\mu(p)$ is given by Eq. (13).

C. Spherical crystals

Spherical crystals have many properties not shared by planar ones, one of the most remarkable being that there is an excess of 12 positive (fivefold) disclinations. These disclinations repel, and the simplest spherical crystals will be those having the minimum number of defects (12) located at the vertices of an icosahedron. Triangular lattices on the sphere with an icosahedral defect pattern are classified by a pair of integers (n,m), as illustrated in Fig. 1. The path from one disclination to a neighboring disclination for an (n,m) icosadeltahedral lattice consists of n straight steps, a subsequent 60° turn, and m final straight steps. The geodesic distance between nearest-neighbor disclinations on a sphere of radius R is $d=R\cos^{-1}(1/\sqrt{5})$. The total number of particles M on the sphere described by this (n,m)-lattice is given by[11]

$$M = 10(n^2 + m^2 + nm) + 2. \qquad (15)$$

Such (n,m) configurations are believed to be low energy states (but not always ground states) for relatively small numbers of M interacting through a Coulomb potential.[38,39,41–43] The energy of discrete particle arrays described by Eq. (5) can be evaluated by starting with some configuration close to an (n,m) one and relaxing it to find a minimum. It is found that the (n,m) configurations are always local minima. Whether these icosahedral configurations are global minima as well will be analyzed later. Results for the energy $E(M)$ are shown in the inset to Fig. 2.

From Fig. 2 it is clear that energies grow very fast for increasing volume. More interestingly, the $(n,0)$ and (n,n) configurations show a growing difference in energy for increasing volume size, implying that the energy of icosahedral configurations does not tend to a universal value for large numbers of particles but rather remains sensitive to the (n,m) configuration, a result also noted by other authors.[19,39]
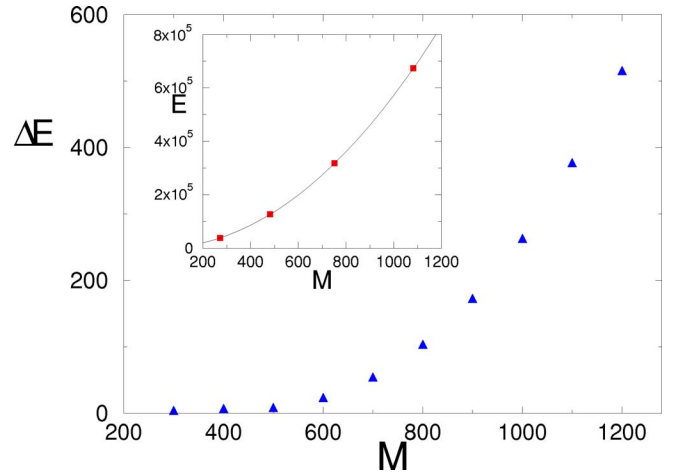

FIG. 2. (Color online) Difference in energy of (n,n) and $(n,0)$ configurations. As the number of particles in the two configurations is always different (at least for relatively small n), we fitted the energy dependence on the number of particles for the two configurations, and then we computed the energy difference from the fitting curves. The energies are plotted in the inset to give an idea of the relative scale of the energy difference. Results are for a power-law potential with $\gamma=1.5$ and energies are plotted in units of e^2/R^γ.

Further insight comes from investigating the distribution of energy. Plots of the local electrostatic energy, the electrostatic energy at point **x** on the sphere, as defined in Eq. (5) are shown in Fig. 3. [40]

From Fig. 3 it should be noted that the triangles obtained by the Voronoi-Delaunay construction, after minimization of the potential Eq. (5), are very close to equilateral.

The distribution of the local energies for the $(n,0)$ and (n,n) configurations are very different. The $(n,0)$ configuration shows maximum energies along the paths joining the defects. The (n,n) configuration, on the other hand, has its maximum energies along the directions defined by the triangles formed by three nearest-neighbor disclinations. The size of these regions of differing electrostatic energy turns out to scale with system size, making it very plausible that there might be small differences in the energy per particle for $(n,0)$ and (n,n) configurations in the limit $n\to\infty$. This point will be discussed in more detail in the following sections.

III. THE GEOMETRIC APPROACH

The minimization of functional forms like Eq. (5) is hampered by the computational complexity of the problem, which is exponential in the particle number for spherical crystals.[41] This difficulty, which is made worse by the "geometric frustration" associated with packing particles on the sphere, limits direct approaches to minimizing the energy to systems having a small number of particles, even if much larger computer resources become available.

One way to overcome these difficulties is to substantially reduce the number of degrees of freedom that need to be considered. An approach focusing on the topological defects as degrees of freedom, rather than on the actual particles, was proposed in Refs. 21 and 45. Some aspects of this for-
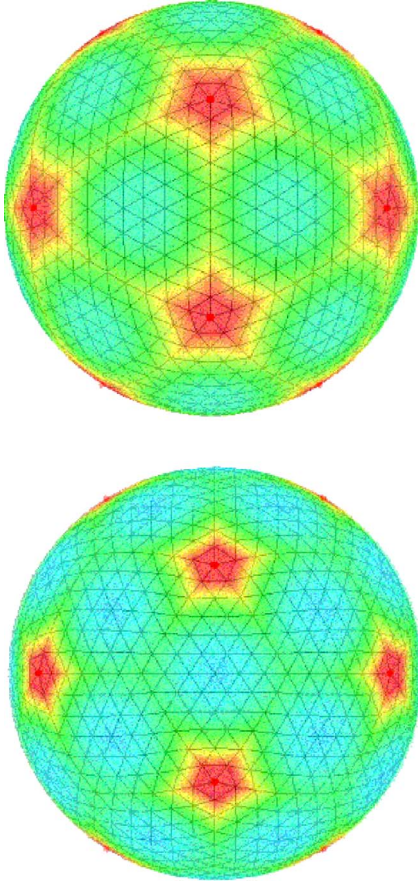
$$\frac{1}{\Delta^2}\rho(\mathbf{x}) = \int d^2\mathbf{x}\sqrt{g}\left(\frac{1}{\Delta^2}\right)_{\mathbf{x},\mathbf{x}'}\rho(\mathbf{x}'). \quad (17)$$

A similar expression can be defined for $(1/\Delta)\rho(\mathbf{x})$ $=(1/\nabla^2)\rho(\mathbf{x})$. Here, $G(\mathbf{x},\mathbf{x}') \equiv (1/\Delta^2)_{\mathbf{x},\mathbf{x}'}$ is a shorthand notation for a Green's function which obeys $\nabla^2 G(\mathbf{x},\mathbf{x}') = \sqrt{g}\delta(\mathbf{x}-\mathbf{x}')$, where ∇^2 is the covariant Laplacian. Positive and/or negative disclinations are attracted to positive and/or negative curvature regions, respectively. We note that at finite temperature, an additional term proportional to

$$\left(K\Big|\frac{1}{\Delta}K\right), \quad (18)$$

arises from the short distance behavior of the measure (the Liouville anomaly).[46] This term can be safely ignored in the present analysis which focuses on zero temperature.

The defect part of the free energy Eq. (16) will be used in a simplified form in the crystalline phase. In that phase the hexatic term can be incorporated into a core energy contribution proportional to the total number of defects. The energy we need to minimize becomes

$$E = E_0 + \frac{Y}{8}\left(\rho\Big|\frac{1}{\Delta^2}\rho\right) + NE_c, \quad (19)$$

where N is the total number of disclinations of core energy E_c.

If the disclination density were continuous, instead of being composed of discrete objects, configurations of defects such that

$$\rho = 0 \Rightarrow s(\mathbf{x}) = K(\mathbf{x}), \quad (20)$$

would be absolute minima of the free energy Eq. (19). In general, defects tend to arrange themselves on curved surfaces to screen the Gaussian curvature as efficiently as possible consistent with their discrete topological charges.

The free energy just discussed can also be applied to *fluctuating* geometries, as in the case of fluid or hexatic membranes (see Refs. 49–52 for reviews). If Young's modulus vanishes, corresponding to a proliferation of unbound dislocations, one obtains the free energy of a hexatic membrane.[46,54,55]

IV. GEOMETRIC FORMALISM ON THE SPHERE

Spherical substrates provide the simplest example of the problem of crystals on curved surfaces. The study of spherical crystals is simplified by two important properties: there is a unique scale with dimensions of length, the radius R, and there is a fixed excess disclinicity of 12 following from the Gauss-Bonnet theorem

$$\int d^2\mathbf{x}\sqrt{g(\mathbf{x})}s(\mathbf{x}) = 4\pi \rightarrow \sum_{i=1}^{N} q_i = 12. \quad (21)$$

The free energy Eq. (19), applied to the sphere, is tractable analytically because the inverse square-Laplacian operator on a sphere of radius R can be computed explicitly. It is shown in Ref. 21 that the Green's function for the square

FIG. 3. (Color online) Potential energy distribution for a $(n,0)$ configuration with $n=10$ and $M=1002$ (top) and a (n,n) configuration with $n=6$ and $M=1082$ (bottom).

malism are now described. The conceptual issues and developments presented in this section are applicable to crystals in any topography. Some of the results given here have already appeared in brief form in Ref. 37.

A. Effective free energy

The elastic energy of a curved crystal may be obtained by writing in a parametrization-invariant way the results for a flat crystal. If the metric of the curved surface is $g_{\alpha\beta}$ (with determinant g), the energy reads

$$\mathcal{H}/T = E_0 + \frac{Y}{8}\left(\rho\Big|\frac{1}{\Delta^2}\rho\right) + \frac{K_A}{2}\left(\rho\Big|\frac{1}{\Delta}\rho\right) + E_s a^2(s|s), \quad (16)$$

where E_0 is the energy of a defect-free monolayer, $(A|B) = \int d^2\mathbf{x}\sqrt{g}AB$, $\rho(\mathbf{x}) = K(\mathbf{x}) - s(\mathbf{x})$ with $K(\mathbf{x})$ the Gaussian curvature and $s(\mathbf{x})$ the disclination density $s(\mathbf{x}) = (\pi/3\sqrt{g})\Sigma_{i=1}q_i\delta(\mathbf{x}-\mathbf{x}_i)$. Here Y is a Young's modulus and K_A is a hexatic stiffness constant. We have added a core energy term to account for the short-distance physics of disclination defects. The quantity $(1/\Delta^2)\rho(\mathbf{x})$ has the meaning

Laplacian, in spherical coordinates (θ, ϕ), has the following simple form on a unit sphere:

$$\chi(\theta^a, \phi^a; \theta^b, \phi^b) = 1 + \int_0^{1-\cos\beta/2} dz \frac{\ln z}{1-z}, \qquad (22)$$

where β is the geodesic distance between two disclinations located at (θ^a, ϕ^a) and (θ^b, ϕ^b),

$$\cos\beta = \cos\theta^a \cos\theta^b + \sin\theta^a \sin\theta^b \cos(\phi^a - \phi^b). \quad (23)$$

The total energy of a spherical crystal with an arbitrary number of disclinations follows from Eq. (19) and (22) and has the simple form[21,63]

$$2E(Y) = E_0 + \frac{\pi Y}{36} R^2 \sum_{i=1}^N \sum_{j=1}^N q_i q_j \chi(\theta^i, \phi^i; \theta^j, \phi^j) + NE_c, \qquad (24)$$

where $\{\theta_i, \phi_i\}_{i=1,\cdots,N}$ are the coordinates of N defects and we restrict ourselves to fivefold ($q_i = +1$) and sevenfold ($q_i = -1$) defects. The quantity E_0 is the zero point energy and is defined in Eq. (6). Although fivefold and sevenfold disclinations will in general have different core energies,[56] we assume equal core energies here for simplicity. What matters for our calculations in any case is the *dislocation* core energy E_d, which we take to be $E_d = E_5 + E_7 \equiv 2E_c$.

The value of the Young's modulus and the flat space ground state energy E_0 have been computed in Sec. II A. When the sphere radius R is large compared to the particle spacing a, we can use flat space values of Y and the flat space energy $E_0(M)$ associated with a finite number of particles M. To obtain the leading terms in the expansion of the ground state energy for large but finite M, the precise compactification of the plane employed is irrelevant—it may be achieved by periodic boundary conditions, for example. For a sufficiently large plane the finite size effects will be negligible. The density σ of particles is then M divided by the total surface of the compact plane, taken to be the surface area of the sphere of radius R,

$$\sigma = 1/A_C = \frac{M}{S}, \quad S = 4\pi R^2. \qquad (25)$$

From Eq. (13) the expression for the Young's modulus suitable for M particles on a spherical crystal of radius R with $0 < \gamma < 2$ is then

$$Y = 4\mu = \frac{4\eta(\gamma)M^{1+\gamma/2}}{(4\pi)^{1+\gamma/2}} \frac{e^2}{R^{2+\gamma}}. \qquad (26)$$

One remaining detail is the divergent contribution to the energy E_0 in Eq. (6). Since the divergent part comes solely from the zero mode, the spatial variations in the density of the actual distribution are irrelevant. It may therefore be computed for a uniform density of charges. The divergent part is identical to the energy of a constant continuum of charges as described by the density Eq. (25). We now evaluate this divergent part of the energy on a sphere, instead of a plane,

$$E_D \equiv Me^2 \frac{\pi}{A_C} \frac{\Gamma\left(1 - \frac{\gamma}{2}\right)}{\gamma/2} \lim_{\vec{G}\to\varepsilon} \frac{2^{2-\gamma}}{|\vec{G}|^{2-\gamma}}$$

$$\to \int \sqrt{g}(\mathbf{x})\rho(\mathbf{x}) \frac{e^2}{|\mathbf{x} - \mathbf{x}'|^\gamma} \rho(\mathbf{x}')\sqrt{g}(\mathbf{x}') = \frac{M^2}{2^{\gamma-1}(2-\gamma)} \frac{e^2}{R^\gamma}. \qquad (27)$$

The divergent part has thus been regularized, and the energy is finite and well defined for all $M < \infty$.

Note that for the case $\gamma < 2$ of primary interest to us here, $E_D \sim M^{2-\gamma/2}(M/S)^{\gamma/2}$. Hence E_D is not simply a function of the particle density M/S, as one would expect for a short-range interaction.

A. The energy of spherical crystals

Upon substituting the elastic constant of Eq. (26) into Eq. (24), one arrives at

$$2E = E_0 + \frac{\pi Y}{36} R^2 \sum_{i=1}^N \sum_{j=1}^N q_i q_j \chi(\theta^i, \varphi^i; \theta^j, \varphi^j) + NE_c$$

$$= E_0 + \frac{4\eta(\gamma)}{(4\pi)^{1+\gamma/2}} \frac{\pi}{36} C(i_1 \cdots i_N) M^{1+\gamma/2} \frac{e^2}{R^\gamma} + NE_c, \qquad (28)$$

where E_0 is defined in Eq. (6) and the function $C(i_1 \cdots i_N)$ depends on the position $i_1 = (\theta_1, \phi_1)$, etc., of the N disclination charges and is universal with respect to the potential. The total energy of a spherical crystal, including the contributions to E_0 is then

$$2E_{\text{TOT}}(M) = \left[\frac{M^2}{2^{\gamma-1}(2-\gamma)} + \left(\frac{\theta(\gamma)}{(4\pi)^{\gamma/2}} \right.\right.$$

$$\left.\left. + \frac{4\eta(\gamma)}{(4\pi)^{1+\gamma/2}} \frac{\pi}{36} C(i_1, \ldots, i_N) \right) M^{1+\gamma/2} \right] \frac{e^2}{R^\gamma} + NE_c. \qquad (29)$$

Note that the leading correction to the zero mode energy proportional to M^2 varies as $M^{1+\gamma/2}$, and depends both on the flat space function $\theta(\gamma)$ and on the C-coefficient

$$C(i_1, \ldots, i_N) = \sum_{j=1}^N \sum_{i=1}^N q_i q_j \chi(\theta^i, \psi^j; \theta^j, \psi^j), \qquad (30)$$

associated with a particular configuration of disclinations.

Note that the core energies contribute to the second subleading coefficient. For short-range potentials, such as $\gamma > 2$, the ground energy is extensive, and the leading term varies as $M^{1+\gamma/2}$.

The extensive nature of the $M^{1+\gamma/2}$ term becomes clear upon noting that

$$M^{1+\gamma/2} \frac{e^2}{R^\gamma} \propto R^2 \times \frac{e^2}{a^{\gamma+2}}, \qquad (31)$$

where a is the particle spacing. Comparison with Eq. (24) shows that the dimension of Young's modulus Y arises solely

from the lattice constant a and the electric charge e, consistent with elastic constants arising from physics on the scale of the lattice constant in an essentially flat geometry. This observation is now generalized to the rest of the couplings discussed in the preceding section.

For the hexatic term, in Eq. (16), we have

$$\frac{K_A}{2}\left(\rho\left|\frac{1}{\Delta}\rho\right.\right) \sim K_A R^0 \sim \frac{e^2}{a^\gamma} \sim M^{\gamma/2}\frac{e^2}{R^\gamma}. \quad (32)$$

Since core energies arise as short-distance divergence's similar to the hexatic term, they are a subleading contribution. For a fluid membrane not on a frozen topography, Helfrich terms arising from the extrinsic curvature $H(\vec{\mathbf{x}})$ as well as the Gaussian curvature can be important. These scale in a way similar to the hexatic term,

$$\kappa\int d\mathbf{x}\sqrt{g}\vec{H}^2 \sim \kappa\int d\mathbf{x}\sqrt{g}\frac{1}{R^2} \equiv \kappa R^0 \sim M^{\gamma/2}\frac{e^2}{R^\gamma},$$

$$\kappa_G\int d\mathbf{x}\sqrt{g}K(\mathbf{x}) \sim \kappa\int d\mathbf{x}\sqrt{g}\frac{1}{R^2} \equiv \kappa R^0 \sim M^{\gamma/2}\frac{e^2}{R^\gamma}. \quad (33)$$

Both terms would therefore contribute to the same order in the M expansion as the hexatic term, although the last term is purely topological. For crystals embedded in a frozen topography we expect an expansion along the lines of Eq. (29),

$$2E_{\text{TOT}}(M) = \left(a_0 M^2 - \sum_{i=1} a_i M^{\gamma/2+1-i}\right)\frac{e^2}{R^\gamma}. \quad (34)$$

The nonextensive term $a_0 M^2$ arises from the long-range interactions. The next extensive contribution comes from the interaction between Gaussian curvature and defects as well as the extensive energy per particle in flat space. Hexatic terms and bending rigidity contributions are higher order in $1/M$ and can be absorbed into a redefinition of the disclination core energy. Core energies also depend on nonuniversal details of the short-distance physics. Core energies are included explicitly in Eqs. (19) and (29).

The results presented so far are strictly for systems at zero temperature. In systems with short-range interactions, the elastic constants can be strongly temperature dependent. An extreme example is hard disks of radius a_0, which may be viewed as a limiting case of a power-law potential of the form $V(r) \simeq \epsilon_0(a_0/r)^\gamma$, with $\gamma\rightarrow\infty$. In this case, the elastic constants are strictly proportional to temperature. It is straightforward, however, to adapt the techniques of this paper to the simpler problem of short-range pair potentials.

B. Energies of icosahedral configurations

The configuration on a sphere with the minimum number of charge ± 1 defects is 12 $+1$ (5-valent) disclinations, which minimize their energy by sitting at the vertices of an icosahedron $\mathcal{Y}$. The energies of such configurations will be computed for the discrete spherical tessellations described in Sec. II C and compared with the predictions of continuum elastic theory, as illustrated in Fig. 4. It is well established that for
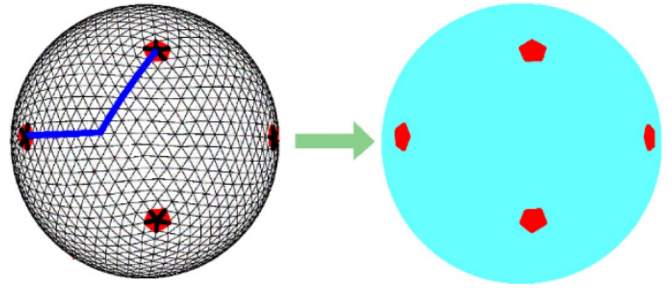

FIG. 4. (Color online) Illustration of the calculation done in the text. The energy of the discrete (n,n) configuration on the left-hand side is extrapolated for large M and compared to the energy computed with the continuum model on the right-hand side. While in the continuum model only 12 degrees of freedom (the 12 disclinations) need to be considered, the direct calculation of a family of discrete models requires the consideration of the full lattice and a careful extrapolation of the energies to large M.

sufficiently large values of M configurations with more than 12 disclinations (i.e., those with "grain boundary scars") have lower energies.[18,19,21] It is of interest, however, to study simple icosahedral configurations for large M, as metastable states with a well-defined energy.

Within the continuum elastic theory it can be shown that 12 disclinations at the vertices of an icosahedron minimize the energy[21] when no further defects are allowed. The C-coefficient of Eq. (29) for this configuration of defects has been computed in[21,64]

$$C(\mathcal{Y}) = 0.6043. \quad (35)$$

$\mathcal{Y}$ here stands for a particle configuration with 12 defects at the vertices of an icosahedron. Using the energy of Eq. (29), the coefficient $a_1(\gamma,\mathcal{Y})$ appearing in the expansion of Eq. (34) may be computed, with the results shown in Fig. 5 and Table II.

From the results described in Sec. II C, the a_1 coefficient may be extrapolated to very large numbers of particles using the expansion derived from Eq. (34). Indeed, as shown in Fig. 6, plots of

$$\epsilon(M) \equiv \frac{2R^\gamma E_{\text{TOT}}(M)/e^2 - a_0(\gamma)M^2}{M^{1+\gamma/2}} \quad (36)$$

vs $1/M$ are linear, with a slope that determines $a_1(\gamma)$ and an intercept related to the higher order core energylike contribution. The results of these extrapolations are shown in Table II. The agreement between the continuum elastic theory and the explicit computation for the (n,n) configuration is remarkable, holding to almost five significant figures. For the $(n,0)$ lattice there is agreement to four significant figures. This agreement is even more striking when it is recalled that the a_1 coefficient is obtained after subtraction of the term $a_0(\gamma)M^2$, as illustrated in Fig. 2. Furthermore, in the range from $\gamma=0.125$ to $\gamma=1.875$, all the significant digits vary and yet the accuracy of the calculation is virtually independent of γ.
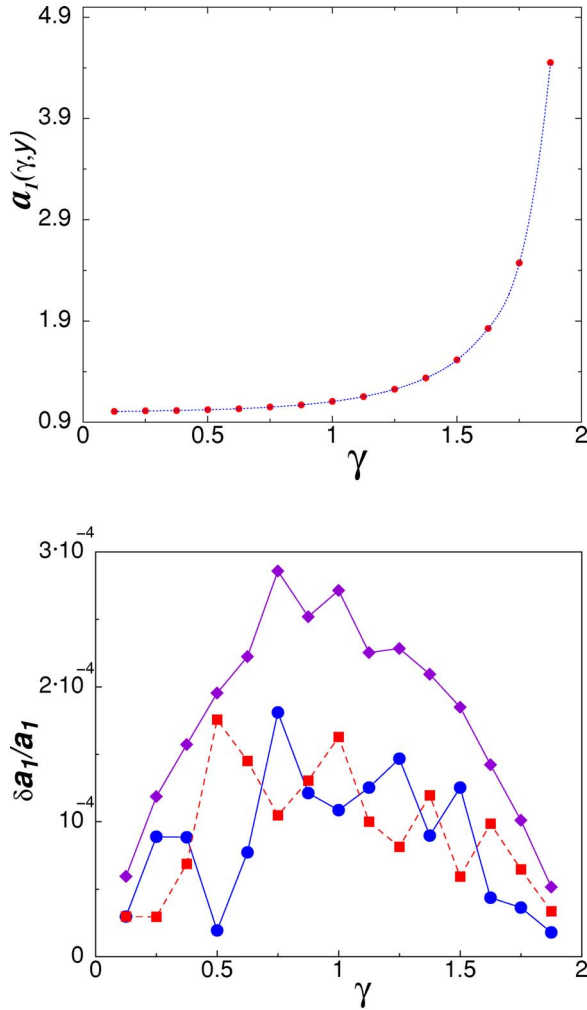
TABLE II. Numerical values of the coefficient $a_1(\gamma, \mathcal{Y})$ (12 disclinations on the vertices of an icosahedron) using the C-coefficient from Eq. (35). The same coefficients from the (n,n) and $(n,0)$ lattices.

γ	$a_1(\gamma, \mathcal{Y})$	(n,n)	$(n,0)$
1.875	4.45118	4.45110(4)	4.45095(4)
1.75	2.47175	2.47166(3)	2.47150(3)
1.625	1.82629	1.82621(2)	1.82603(2)
1.5	1.51473	1.51454(2)	1.51445(2)
1.375	1.33695	1.33683(4)	1.33667(4)
1.25	1.22617	1.22599(7)	1.22589(7)
1.125	1.15366	1.1535(2)	1.15340(2)
1.0	1.10494	1.10482(3)	1.10464(3)
0.875	1.07187	1.07174(3)	1.07160(3)
0.75	1.04940	1.04921(6)	1.04910(6)
0.625	1.03421	1.03413(5)	1.03398(5)
0.5	1.02392	1.02390(4)	1.02372(4)
0.375	1.01672	1.01663(6)	1.01656(6)
0.25	1.01115	1.01106(3)	1.01103(3)
0.125	1.00595	1.00592(2)	1.00589(2)

The formal elimination of the geometric frustration introduced by the Gaussian curvature may be formulated as a concrete set of equations in the case of the sphere. We shall use the identity
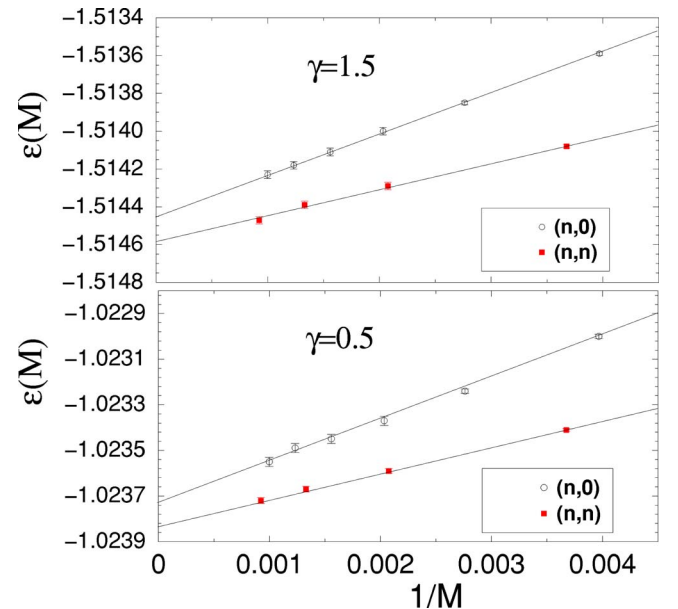
FIG. 5. (Color online) Energy coefficient a_1 as a function of gamma (solid line) and from the numerical results with (n,m) configurations (filled circles), for the icosahedral configurations. Plot of $a_1(\gamma,\mathcal{Y}) - a_1(\gamma,\mathcal{Y})^{(n,n)}$ (circles), $a_1(\gamma,\mathcal{Y}) - a_1(\gamma,\mathcal{Y})^{(n,0)}$ (diamonds), $a_1(\gamma,\mathcal{Y})^{(n,n)} - a_1(\gamma,\mathcal{Y})^{(n,0)}$ (squares).

C. The energy difference of the (n,m) lattices

The a_1 coefficient computed within our continuum elastic approach above does not depend on the icosadeltahedral class (n,m). Results from the direct minimization of particles do, however, show a weak dependence (in the fourth significant digit) on the particular (n,m) configuration, as is apparent from Fig. 2 and Table II. It should be noted that the discrepancy from the continuum result has a well-defined sign, and is therefore reasonably attributed to a term not present in the energy expansion.

V. THOMSON PROBLEM WITH A CONTINUOUS DISTRIBUTION OF DISLOCATIONS

When the number of particles is extremely large, the minimum energy configurations can be approximated by a closed analytical form, upon assuming a continuous distribution of defects. Only the sphere will be worked out here, but other curved surfaces can be treated in a very similar fashion.

FIG. 6. (Color online) Numerical estimate of $\varepsilon(M)$ as a function of $1/M$ for $(n,0)$ and (n,n) icosadeltahedral lattices with $\gamma = (1.5, 0.5)$.

TABLE III. Value of the a_1 coefficients for the $\mathcal{G}$ configuration Eq. (38).

γ	$a_1(\gamma,\mathcal{G})$	γ	$a_1(\gamma,\mathcal{G})$	γ	$a_1(\gamma,\mathcal{G})$	γ	$a_1(\gamma,\mathcal{G})$
1.875	4.45227	0.875	1.07297	1.75	2.47289	0.75	1.05044
1.625	1.82746	0.625	1.03515	1.5	1.51592	0.5	1.02473
1.375	1.33815	0.375	1.01737	1.25	1.22737	0.25	1.01161
1.125	1.15485	0.125	1.00620	1	1.10610		

$$s(\mathbf{x}) = \frac{\pi}{3\sqrt{g}}\sum_{i=1}^{N} q_i \delta(\mathbf{x},\mathbf{x}_i)$$

$$= \frac{1}{R^2} + \frac{\pi}{3R^2}\sum_{l=1}^{\infty}\sum_{m=-l}^{l} Y_m^{l*}(\theta,\phi)\sum_{i=1}^{N} q_i Y_m^{l*}(\theta_i,\phi_i)$$

$$= K(\mathbf{x}) + \frac{\pi}{3R^2}\sum_{l=1}^{\infty}\sum_{m=-l}^{l} Y_m^{l*}(\theta,\phi)\sum_{i=1}^{N} q_i Y_m^{l}(\theta_i,\phi_i), \quad (37)$$

which follows from the topological constraint Eq. (21). Provided a disclination configuration exists such that

$$\sum_{i=1}^{N} q_i Y_m^{l}(\theta_i,\phi_i) = 0, \quad (38)$$

for each ($l \geq 1, m$), the disclination density completely screens the Gaussian curvature. A configuration of defects satisfying Eq. (38) is an absolute minimum of the elastic energy, a result easily understood by writing the energy in the form

$$E = E_0 + \frac{\pi^2 Y}{9}R^2 \sum_{l=1}^{\infty}\sum_{m=-l}^{l} \frac{\left|\sum_{i=1}^{N} q_i Y_m^{l}(\theta_i,\phi_i)\right|^2}{l^2(l+1)^2} + N E_c, \quad (39)$$

where the zero point energy E_0 in Eq. (16) is kept. A configuration satisfying Eq. (38) will be denoted by $\mathcal{G}$. (See Table III.) For this hypothetical configuration, the C-coefficient in Eq. (29) vanishes, although there is now a large contribution (linear in R) from the dislocation core energies represented by the last term of Eq. (39).

The $\mathcal{G}$ configuration may be characterized more explicitly. It consists of a density of dislocations that converges to the local Gaussian curvature. It can be shown that upon approximating the dislocations (each regarded as a disclination dipole with spacing a) as a continuum distribution, this dislocation density for a sphere becomes

$$\vec{b}(\theta,\varphi) = \frac{1}{6R}\sum_{k=1}^{6} \cot[\alpha_k(\theta,\varphi)]e_\varphi^k. \quad (40)$$

The summation here runs over the six coordinates of the northern hemisphere of an icosahedron $((0,0)$ and $(\theta_y, 2\pi k/5)$, where $\theta_y = \arccos(1/\sqrt{5})$ and α_k is the angle θ relative to a coordinate system with the north pole located at $(\theta_y, 2\pi k/5)$ for $k=1,\dots,5$. This angle is given implicitly by

$$\cos[\alpha_k(\theta,\varphi)] = \cos(\theta)\cos(\theta_y) - \sin(\theta)\sin(\theta_y)\cos\left(\frac{2\pi}{5}k + \varphi\right). \quad (41)$$

The implicit form of Eq. (40) can be further simplified

$$\vec{e}_\varphi^k = f^k(\theta,\varphi)\left\{-\sin(\theta_y)\sin\left(\frac{2\pi}{5}k + \varphi\right)\vec{e}_\theta \right.$$
$$\left. + \left[\{\cos(\theta_y)\sin\theta + \sin(\theta_y)\}\cos\theta\cos\left(\varphi + \frac{2\pi}{5}k\right)\right]\vec{e}_\varphi\right\}, \quad (42)$$

where $f^k(\theta,\varphi) = 1/\sin(\alpha_k(\theta,\varphi))$.

Close to one of the 12 disclinations with charges $=+2\pi/6$ Eq. (40) predicts a singularity in the dislocation density[45]

$$b \approx \frac{s}{2\pi R a}. \quad (43)$$

For small angles, close to each disclination, there is a short-distance singularity

$$b(\theta) = \frac{\pi}{3R\theta} + \cdots , \quad (44)$$

in agreement with known results in flat space.

Equation (40) represents a continuous distribution of dislocations, and neglects both dislocation discreteness and their mutual interactions. It represents six families of dislocations with azimuthal Burgers' vectors associated with antipodal pairs of the 12 original disclinations in the icosahedron. When discreteness and interactions are taken into account, we expect these dislocations to condense into grain boundary arms containing quantized Burgers' vectors and variable spacing in the radial direction.[21,44] This discrete solution consists of five radial grain boundaries from each of the 12 icosadeltahedral configurations, with dislocations having a variable spacing that is determined from the condition that the resulting spherical tessellation, defined by both the regular and defected sites, is made of optimally close to equilateral triangles, thus determining a configuration whose C-coefficient asymptotically approaches the C-coefficient of a planar configuration, which is obviously zero.[57] Numerical verifications for the vanishing of the C-coefficient have been provided in Ref. 36. It should be noted that the discrete solution presented in Ref. 57 still shows some degeneracy such as the number of radial arms from each disclination.
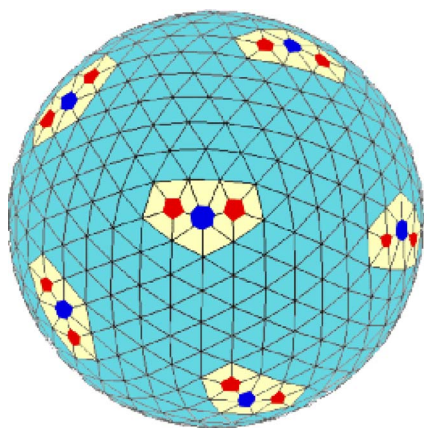
FIG. 7. (Color online) Results of a minimization of 500 particles interacting with a Coulomb potential, showing the appearance of scars.

A. The intermediate regime

Within the continuum elastic approach, the dominant configurations for a small number of particles are 12 defects with an icosahedral symmetry.[21] We have just seen, however, that adding a continuous distribution of dislocations, as might be appropriate when the particle number is large, can more efficiently screen the Gaussian curvature on a sphere. The natural problem then becomes to determine the precise structure of the defect arrays for intermediate numbers of particles when the discreteness of interacting dislocations is taken into account.

We note first that the particular arrangement of defects dominating in this regime will not be fully universal. The particular array structure favored can vary from system to system with fixed particle number, depending, e.g., on details such as the dislocation core energy. This result may be traced back to the M-expansion of Eq. (34), in which the subleading terms which depend on nonuniversal properties influence the dominant terms for finite values of M. Some typical defect configurations obtained by direct minimization of particles on the sphere are shown in Fig. 7 and show incipient scars, already at number of particles of 500 (in Refs. 21 and 53 the minimum number of particles where scars are systematically found is predicted around 400). By using the geometrical model described in this paper, where the energy is parametrized just by a Young's modulus and a dislocation core energy[21,22] one can simulate larger particle numbers and one obtains results as in Fig. 8. Note the occurrence of low energy configurations with scars ($m=2$) in one instance and pentagonal buttons ($m=5$) in another. The dislocation spacing decreases the further a dislocation is from the central disclination.

An overview of previous results involving grain boundary scars is presented in Fig. 9. If a disclination is placed on a perfect crystal, no additional defects will appear if the disclination is located on the tip of a cone with total Gaussian curvature equal to the disclination charge. If a disclination is forced into a flat monolayer, then m low angle grain boundaries, with constant spacing between dislocations as shown in Fig. 9 and grains going all the way to the boundary, will
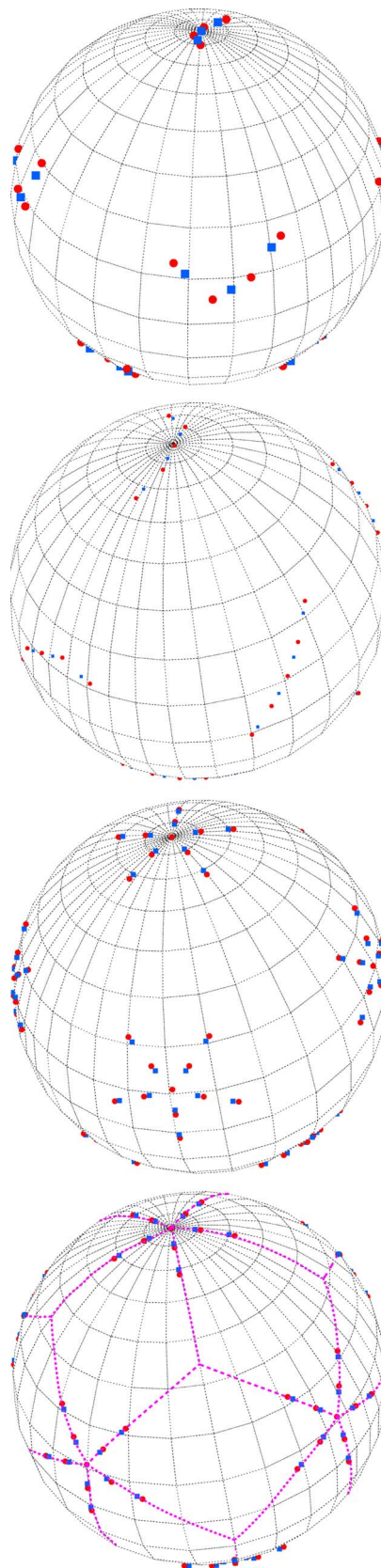

FIG. 8. (Color online) Ground state configurations for M ≈ 2000 particles obtained from the continuum elastic formalism. In the top figure one finds scars ($m=2$) and in the bottom pentagonal buttons ($m=5$) forming a rhombic tricontahedron.
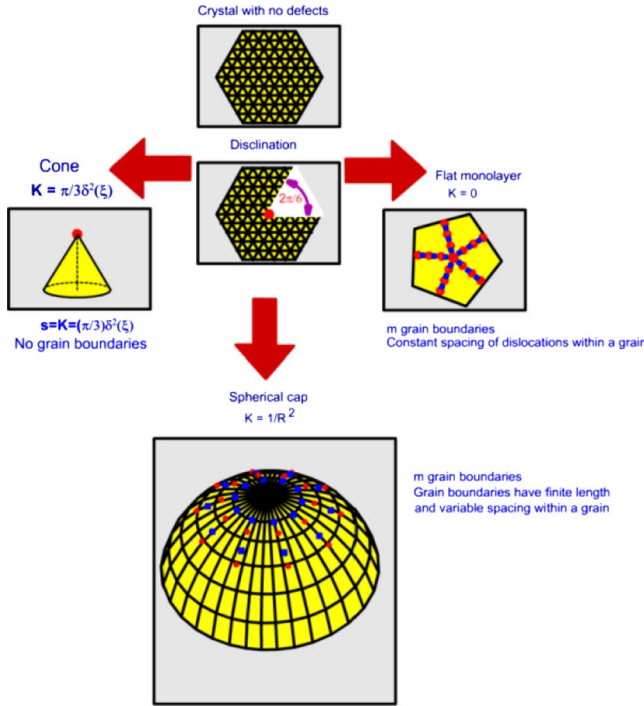
FIG. 9. (Color online) Schematic illustrating the genesis of grain boundary scars. A disclination is first constructed from a perfect lattice. If this disclination is placed on a tip of a cone, with a delta function of Gaussian curvature balancing the defect charge, then no additional defects form. If the crystal is forced into a monolayer, grain boundaries radiating out of the disclination radiate all the way to the boundary. In the intermediate regime of constant nonzero Gaussian curvature, m grain boundaries of finite length and variable spacing of dislocations form.

be favored (see Ref. 44 for a detailed discussion). In the intermediate situation where a finite Gaussian curvature is spread over a finite area, as in the case of a spherical cap, a disclination arises at the center of the cap, and finite length grain boundaries stretched out over an area of $(\pi/3)R^2$ with variable spacing dominate, again as illustrated in Fig. 9. Since several nonuniversal features, related to the size of the core energies, commensurability properties and so on, will have an important effect in this regime of M, the previous argument should describe the general trends and will be realized in an approximate form only.

Additional results may be obtained for the number of arms within the grain boundary, the actual variable spacing between dislocations within the grain and the length of the grains as a function of the number of particles. The detailed study of these questions will be reported elsewhere.

When grain boundary scars appear, we can estimate the number of excess dislocations which decorate each of the 12 curvature-induced disclinations on the sphere using ideas from Ref. 21. This estimate is in reasonable agreement with experiments probing equilibrated assemblies of polystyrene beads on water droplets.[22] Consider the region surrounding one of the 12 excess disclinations, with charge $s=2\pi/6$, centered on the north pole. As discussed in Ref. 21, we expect the stresses and strains at a fixed geodesic distance r from the pole on a sphere of radius R to be controlled by an *effective* disclination charge

$$s_{\text{eff}}(r) = s - \int_0^{2\pi} d\phi \int_0^r dr' \sqrt{g(r)} K = \pi/3 - 4\pi \sin^2\left(\frac{r}{2R}\right).$$

(45)

Here the Gaussian curvature is $K = 1/R^2$ and the metric tensor associated with spherical polar coordinates (r, ϕ), with distance element $ds^2 = d^2r + R^2 \sin^2(r/R)d^2\phi$, gives $\sqrt{g(r)} = R \sin(r/R)$. Suppose m grain boundaries radiate from the disclination at the north pole. Then, in an approximation which neglects interactions between the individual arms, the spacing between the dislocations in these grains is[21]

$$l(r) = \frac{am}{s_{\text{eff}}(r)},$$

(46)

which implies an effective dislocation density,

$$n_d(r) = \frac{1}{l(r)} = \frac{1}{ma}\left(\frac{\pi}{3} - 4\pi \sin^2(r/2R)\right) = \frac{2\pi}{ma}\left(\cos\frac{r}{R} - 5/6\right).$$

(47)

This density vanishes when $r \rightarrow r_c$, where

$$r_c = R \cos^{-1} 5/6 \approx R(33.56°),$$

(48)

which is the distance at which the m grain boundaries terminate. The total number of dislocations residing within this radius is thus

$$N_d = m \int_0^{r_c} n_d(r)dr = \frac{r_c}{a}\frac{\pi}{3} - \frac{4\pi}{a}\int_0^{r_c} \sin^2(r/2R)dr$$

$$= \frac{\pi}{3}[\sqrt{11} - 5\cos^{-1}(5/6)](R/a) \approx 0.408(R/a). \quad (49)$$

As discussed in Ref. 37, it is also of interest to consider 2π disclination defects (appropriate to crystals of tilted molecules[59]) on the sphere. The icosahedral configuration of 12 $s = 2\pi/6$ disclinations is now replaced by just two $s = 2\pi$ disclinations at the north and south poles. Using the approximation discussed above, it is straightforward to show that the density of dislocations in each of m (noninteracting) grain boundary arms now reads

$$n_d(r) = \frac{2\pi}{ma}\cos\left(\frac{r}{R}\right).$$

(50)

This density vanishes at $r_c = (\pi/2)R$, corresponding to a hemisphere of area on the sphere for each cluster of arms.

It is of considerable interest to repeat the above calculation for a square lattice, as found, for example, in the protein surface layers (s layers) of some bacteria.[47,48] In this case the basic disclination has $s = 2\pi/4$. The effective dislocation density becomes

$$n_d(r) = \frac{1}{l(r)} = \frac{1}{ma}\left(\frac{\pi}{2} - 4\pi \sin^2(r/2R)\right) = \frac{2\pi}{ma}\left(\cos\frac{r}{R} - 3/4\right).$$

(51)

This density vanishes when $r \rightarrow r_c$, where

$$r_c = R \cos^{-1} 3/4 \approx R(41.4°), \tag{52}$$

which is the distance at which the m grain boundaries terminate. The longer angular length of square lattice scars reflects the larger initial disclination charge (90°) that must be screened. The total number of dislocations residing within this radius is thus

$$N_d = m \int_0^{r_c} n_d(r)dr = \frac{r_c}{a}\frac{\pi}{2} - \frac{4\pi}{a}\int_0^{r_c} \sin^2(r/2R)dr$$

$$= \frac{\pi}{2}[\sqrt{7} - 3\cos^{-1}(3/4)](R/a) \approx 0.75(R/a). \tag{53}$$

Thus the angular length of scars and the total number of excess dislocations is a measure of the underlying topology of the lattice tiling the sphere.

VI. CONCLUSIONS

A. Summary of results

In this section we summarize the most relevant results obtained from the analysis presented earlier.

In Sec. II we treated several properties of planar and spherical crystals which were subsequently used to test our continuum elastic formalism. We computed the energy Eq. (6) and elastic tensor Eq. (9) for triangular lattices in flat space for a general long-range power-law potential of the type Eq. (2). The continuum elastic formalism, where defects such as disclinations and disclination dipoles ≡ dislocations are the relevant degrees of freedom and six-coordinated particles are treated as a continuous elastic background, was discussed in Sec. III. It was shown that the total energy is expressible as an expansion in powers in the total number of particles [Eq. (29)],

$$2E = \left(\frac{M^2}{2^{\gamma-1}(2-\gamma)} - a_1(\gamma|\{q_i\}_{i=1,\dots,N})M^{1+\gamma/2}\right.$$
$$\left. - a_2(\gamma|\{q_i\}_{i=1,\dots,N})M^{\gamma/2}\right)\frac{e^2}{R^\gamma}, \tag{54}$$

where each coefficient has a clear geometric interpretation in terms of continuum results.

Our approach was illustrated for the generalized Thomson problem in Sec. IV. Using the elastic constants computed in flat space, the continuum elastic theory gives concrete energy predictions, with no fitting parameters, as a series expansion in the total number of particles M, which can be compared with the energies obtained numerically for spherical crystals. We find agreement to five significant figures for (n,n) icosadeltahedral lattices and to four significant figures for $(n,0)$ lattices, as presented in Table II. Only a small discrepancy, of order the difference between $(n,0)$ and (n,n) tessellations, separates the continuum results from results for actual spherical crystals.

The limit of a very large number of particles M was dealt with in Sec. V. A "Debye-Huckel"-type formulation where dislocations are treated in a smeared continuum density of Burgers' vectors was proposed. The actual solution in the large M limit is a discrete version of the continuum solution presented in this paper, and incorporates the discreteness of the dislocation positions and charges and their mutual interactions and has been briefly discussed in Sec. V. A more detailed discussion can be found in Ref. 57. We should mention that an alternative scenario for the Thomson problem has been proposed,[58] where at some finite value of number of particles an instability to a "spontaneously magnetized" state is predicted. Based on the results presented in this paper and in Refs. 36 and 57 we conclude that such instability does not appear for the generalized Thomson problem. It is possible that an instability of the type predicted in Ref. 58 may appear for charges on spheres under other types of constraints.

The intermediate regime was discussed in the preceding section and it was shown that the underlying universality of the result competes with several nonuniversal features of the problem.

B. Outlook

The main goal of this paper was to introduce a continuum elastic approach to address the problem of two-dimensional crystals in frozen topographies. The formalism has been explicitly applied to the sphere, but it appears general enough to be applicable to a variety of other geometries. The case of crystalline order on a torus is currently under exploration.

We hope this presentation will inspire further work on the problem of crystals on curved topographies. The long-range pair interactions on a sphere studied here certainly do not exhaust the possible problems.

APPENDIX A: THE EVALUATION OF POTENTIALS

The details of the computation of the energy and the elastic tensor, Eqs. (6) and (9) are described in detail. The approach followed is a generalization of the one used by Bonsall and Maradudin.[60] See also Ref. 61.

1. Computation of the energy

The energy for a system of M particles located at positions $\vec{R}(\mathbf{1})$ of a 2D Bravais lattice, defined by vectors $\mathbf{a}_i$ and $\mathbf{e}_i$ in direct and reciprocal space

$$\vec{R}(\mathbf{1}) = l_1 \mathbf{a}_1 + l_2 \mathbf{a}_2, \tag{A1}$$

$$\vec{G}(\mathbf{h}) = h_1 \mathbf{e}_1 + h_2 \mathbf{e}_2 \tag{A2}$$

is given by Eq. (5),

$$E_0 = \frac{e^2}{2} \sum_{\mathbf{1} \neq \mathbf{1}'}^{M} \frac{1}{|\vec{R}(\mathbf{1}) - \vec{R}(\mathbf{1}')|^\gamma} = M \frac{e^2}{2} \lim_{\vec{x} \to 0} \sum_{l \neq 0} \frac{1}{|\vec{x} - \vec{R}(\mathbf{1})|^\gamma}$$

$$\equiv \frac{M}{2} E(\gamma). \tag{A3}$$

To efficiently perform the sum (a generalization of the Ewald method), we separate short and long distances contributions, since they give rise to different singular behavior. This may be achieved by the identity Eq. (B1),

$$\frac{1}{|\vec{x} - \vec{R}(\mathbf{1})|^\gamma} = \frac{1}{\Gamma\left(\frac{\gamma}{2}\right)} \left(\int_\sigma^\infty dt\, t^{-1+\gamma/2} e^{-t|\vec{x} - \vec{R}(\mathbf{1})|^2} \right.$$

$$\left. + \int_0^\sigma dt\, t^{-1+\gamma/2} e^{-t|\vec{x} - \vec{R}(\mathbf{1})|^2} \right)$$

$$= \frac{\sigma^{\gamma/2}}{\Gamma\left(\frac{\gamma}{2}\right)} \varphi_{\gamma/2-1}(\sigma|\vec{x} - \vec{R}(\mathbf{1})|^2)$$

$$+ \frac{\sigma^{\gamma/2}}{\Gamma\left(\frac{\gamma}{2}\right)} \int_0^1 dt\, t^{-1+(\gamma/2)} e^{-t\sigma|\vec{x} - \vec{R}(\mathbf{1})|^2}. \tag{A4}$$

The definition of the Misra functions φ_n is given below in Eq. (B2).

Using the Poisson summation formula Eq. (B5), the last term in Eq. (A4) can also be expressed in terms of Misra functions,

$$\sum_l \int_0^1 dt\, t^{-1+\gamma/2} e^{-t\sigma|\vec{x} - \vec{R}(\mathbf{1})|^2} = \frac{\pi}{A_C \sigma} \sum_{\vec{G}} e^{i\vec{G} \cdot \vec{x}} \int_1^\infty dt\, t^{-\gamma/2} e^{-t(|\vec{G}|^2/4\sigma)}$$

$$= \frac{\pi}{A_C \sigma} \sum_{\vec{G}} e^{i\vec{G} \cdot \vec{x}} \varphi_{-\gamma/2}\left(\frac{|\vec{G}|^2}{4\sigma}\right), \tag{A5}$$

where $\vec{G}$ are the vectors in reciprocal space of the Bravais lattice, and A_C is the area of the unit cell.

Upon combining Eqs. (A4) and (A5), the energy Eq. (A3) becomes

$$E(\gamma) = \frac{\sigma^{\gamma/2} e^2}{\Gamma\left(\frac{\gamma}{2}\right)} \sum_{l \neq 0} \varphi_{\gamma/2-1}(\sigma|\vec{x} - \vec{R}(\mathbf{1})|^2) - \frac{2\sigma^{\gamma/2}}{\gamma \Gamma(\gamma/2)} e^2$$

$$+ \frac{\pi e^2 \sigma^{\gamma/2-1}}{A_C \Gamma(\gamma/2)} \sum_{\vec{G}} e^{i\vec{G} \cdot \vec{x}} \varphi_{-\gamma/2}\left(\frac{|\vec{G}|^2}{4\sigma}\right). \tag{A6}$$

Although the limit $\vec{x} \to 0$ is in general convergent, the term

$\vec{G} = 0$ requires special attention. This term must be treated separately by considering $|\vec{G}|$ small but nonvanishing,

$$\frac{\pi e^2 \sigma^{\gamma/2-1}}{\Gamma(\gamma/2)} e^{i\vec{G}\mathbf{x}} \varphi_{-\gamma/2}\left(\frac{|\vec{G}|^2}{4\sigma}\right)$$

$$= \frac{\pi 2^{2-\gamma} \Gamma(1 - \gamma/2)}{|\vec{G}|^{2-\gamma} \Gamma(\gamma/2)} e^2 - \frac{\pi \sigma^{\gamma/2-1}}{A_C \Gamma(\gamma/2)(1 - \gamma/2)} e^2 + O(|\vec{G}|). \tag{A7}$$

Thus, the singularity as $\vec{G} \to 0$, associated with the large distance behavior, has been explicitly isolated.

The results derived so far are completely general, valid for any Bravais lattice. Since only the triangular lattice is relevant to this paper, complete results for other Bravais lattices will be published elsewhere. The two vectors $\mathbf{a}_1$, $\mathbf{a}_2$ defining the triangular lattice in direct space, and the two vectors $\mathbf{e}_1$, $\mathbf{e}_2$ in reciprocal space are taken as

$$\mathbf{a}_1 = (a, 0), \quad \mathbf{e}_1 = \frac{2\pi}{a}\left(1, -\frac{\sqrt{3}}{3}\right),$$

$$\mathbf{a}_2 = \left(\frac{a}{2}, \frac{\sqrt{3}a}{2}\right), \quad \mathbf{e}_2 = \frac{2\pi}{a}\left(0, 2\frac{\sqrt{3}}{3}\right), \tag{A8}$$

where a is the lattice constant. Further simplification is achieved by choosing σ as $\sigma = \pi/A_C$ (where $A_C = \sqrt{3}/2a^2$), so that the argument in the Misra functions has a similar form for the sums in both direct and reciprocal space. Thus,

$$\sigma \vec{R}^2(\mathbf{1}) = \frac{\pi}{A_0}(l_1^2 \mathbf{a}_1^2 + 2l_1 l_2 \mathbf{a}_1 \mathbf{a}_2 + l_2^2 \mathbf{a}_2^2), \tag{A9}$$

$$\frac{\mathbf{G}^2(h)}{4\sigma} = \frac{1}{4\sigma}(h_1^2 \mathbf{e}_1^2 + 2h_1 h_2 \mathbf{e}_1 \mathbf{e}_2 + h_2^2 \mathbf{e}_2^2)$$

$$= \frac{\pi}{A_0}(h_1^2 \mathbf{a}_1^2 - 2h_1 h_2 \mathbf{a}_1 \mathbf{a}_2 + h_2^2 \mathbf{a}_2^2). \tag{A10}$$

Our final form for the energy is then

$$E(\gamma) = -\frac{e^2}{\Gamma(\gamma/2)}\left\{ \left(\frac{\pi}{A_C}\right)^{\gamma/2}\left\{ \frac{4}{\gamma(2 - \gamma)} - \sum_{l \neq 0} \varphi_{-\gamma/2}\left(\frac{\pi}{A_C}\vec{R}^2(\mathbf{1})\right)\right.\right.$$

$$\left.\left. - \sum_{l \neq 0} \varphi_{\gamma/2-1}\left(\frac{\pi}{A_C}\vec{R}^2(\mathbf{1})\right)\right\}\right\}$$

$$+ \lim_{|\vec{G}| \to 0} \frac{\pi 2^{2-\gamma} \Gamma(1 - \gamma/2)}{A_C |\vec{G}|^{2-\gamma} \Gamma(\gamma/2)} e^2. \tag{A11}$$

The summation over the Misra functions is exponentially convergent; just a few terms give a very accurate result.

2. Computation of the elastic tensor

The response function is defined in Eq. (8). Using some simple algebra, the explicit form for this tensor response function Π follows:

$$\Pi_{\alpha,\beta}(\mathbf{1},\mathbf{1}') = \begin{cases} -\gamma(\gamma+2)\dfrac{[\vec{R}(\mathbf{1})-\vec{R}(\mathbf{1}')]_\alpha[\vec{R}(\mathbf{1})-\vec{R}(\mathbf{1}')]_\beta}{|[\vec{R}(\mathbf{1})-\vec{R}(\mathbf{1}')]|^{\gamma+4}} + \gamma\dfrac{\delta_{\alpha\beta}}{|[\vec{R}(\mathbf{1})-\vec{R}(\mathbf{1}')]|^{\gamma+2}}, & \mathbf{1}\neq\mathbf{1}', \\[2mm] -\displaystyle\sum_{l\neq l'}\Pi_{\alpha\beta}(\mathbf{1},\mathbf{1}'), & \mathbf{1}=\mathbf{1}'. \end{cases} \tag{A12}$$

The property $\vec{R}(\mathbf{1})-\vec{R}(\mathbf{1}')=\vec{R}(\mathbf{1}-\mathbf{1}')-\vec{R}(0)$ implies translational invariance $\Pi(\mathbf{1},\mathbf{1}')=\Pi(\mathbf{1}-\mathbf{1}',0)$. The response function is better studied in Fourier space. The Fourier transformed elastic tensor can be computed from the identity

$$\Pi_{\alpha\beta}(\vec{p}) = -[S_{\alpha\beta}(\vec{p})-S_{\alpha\beta}(\vec{0})], \tag{A13}$$

with $S_{\alpha\beta}$ defined as

$$\begin{aligned} S_{\alpha\beta}(\vec{p}) &= \lim_{\vec{x}\to 0}\frac{\partial^2}{\partial_\alpha\partial_\beta}\left(e^{-i\vec{p}\cdot\vec{x}}\sum_{l\neq 0}e^{i\vec{p}[\vec{x}-\vec{R}(\mathbf{1})]}\frac{1}{|\vec{x}-\vec{R}(\mathbf{1})|^\gamma}\right)\\ &= \lim_{\vec{x}\to 0}\frac{\partial^2}{\partial_\alpha\partial_\beta}\mathcal{F}(\vec{x},\vec{p}), \end{aligned}$$

$$\mathcal{F}(\vec{x},\vec{p}) \equiv \sum_l \frac{e^{i\vec{p}\cdot(\vec{x}-\vec{R}(\mathbf{1}))}}{|\vec{x}-\vec{R}(\mathbf{1})|^\gamma}. \tag{A14}$$

The function $\mathcal{F}$ can be computed by further using Eqs. (A4), (A5), and (B5), with essentially the same steps as in previous computations, leading to the expression

$$\begin{aligned} \mathcal{F}(\vec{x},\vec{p}) &= \frac{\sigma^{\gamma/2}}{\Gamma(\gamma/2)}\sum_{l\neq 0}e^{-i\vec{p}\vec{R}(\mathbf{1})}\varphi_{\gamma/2-1}(\sigma|\vec{x}-\vec{R}(\mathbf{1})|^2)\\ &\quad -\frac{\sigma^{\gamma/2}}{\Gamma(\gamma/2)}\int_0^1 dt\, t^{-1+\gamma/2}e^{-t|\vec{x}|^2\sigma}\\ &\quad +\frac{\pi\sigma^{\gamma/2-1}}{A_C\Gamma(\gamma/2)}\sum_{G\neq 0}e^{i(\vec{p}+\vec{G})\cdot\vec{x}}\varphi_{-\gamma/2}\left(\frac{|\vec{p}+\vec{G}|^2}{4\sigma}\right)\\ &\quad +\frac{\pi\sigma^{\gamma/2-1}}{A_C\Gamma(\gamma/2)}\varphi_{-\gamma/2}\left(\frac{|\vec{p}+\vec{G}|^2}{4\sigma}\right). \end{aligned} \tag{A15}$$

Upon inserting the derivatives of the Misra functions obtained from Eq. (B3) and (B4) and using Eq. (A14), we have

$$\begin{aligned} S_{\alpha\beta}(\vec{p}) &= -\frac{\pi\sigma^{\gamma/2-1}}{A_C\Gamma(\gamma/2)}\sum_{\vec{G}}(\vec{p}+\vec{G})_\alpha(\vec{p}+\vec{G})_\beta\varphi_{-\gamma/2}\left(\frac{|\vec{p}+\vec{G}|^2}{4\sigma}\right)\\ &\quad -\frac{2\sigma^{\gamma/2+1}}{\Gamma(\gamma/2)}\sum_{l\neq 0}e^{-i\vec{p}\cdot\vec{R}(\mathbf{1})}\varphi_{\gamma/2}(\sigma|\vec{R}(\mathbf{1})|^2)\\ &\quad -\frac{4\sigma^{\gamma/2+2}}{\Gamma(\gamma/2)}\sum_{l\neq 0}\vec{R}(\mathbf{1})_\alpha\vec{R}(\mathbf{1})_\beta\varphi_{1+\gamma/2}(\sigma|\vec{R}(\mathbf{1})|^2) \end{aligned}$$

$$+\frac{4}{2+\alpha}\frac{\sigma^{\gamma/2+1}}{\Gamma(\gamma/2)}. \tag{A16}$$

The full expression for the response function is then

$$\begin{aligned} \Pi_{\alpha\beta}(\vec{p}) &= \frac{\pi\sigma^{\gamma/2-1}}{A_C\Gamma(\gamma/2)}\sum_{\mathbf{G}}(\vec{p}+\vec{G})_\alpha(\vec{p}+\vec{G})_\beta\varphi_{-\gamma/2}\left(\frac{|\vec{p}+\vec{G}|^2}{4\sigma}\right)\\ &\quad -\frac{\pi\sigma^{\gamma/2-1}}{A_C\Gamma(\gamma/2)}\sum_{\vec{G}}\vec{G}_\alpha\vec{G}_\beta\varphi_{-\gamma/2}\left(\frac{|\vec{G}|^2}{4\sigma}\right)\\ &\quad +\frac{2\sigma^{\gamma/2+1}}{\Gamma(\gamma/2)}\sum_{l\neq 0}(e^{-i\vec{p}\cdot\vec{R}(\mathbf{1})}-1)\varphi_{\gamma/2}[\sigma|\vec{R}(\mathbf{1})|^2]\\ &\quad -\frac{4\sigma^{\gamma/2+2}}{\Gamma(\gamma/2)}\sum_{l\neq 0}(e^{-i\vec{p}\cdot\vec{R}(\mathbf{1})}-1)\\ &\quad \times\vec{R}(\mathbf{1})_\alpha\vec{R}(\mathbf{1})_\beta\varphi_{1+\gamma/2}[\sigma|\vec{R}(\mathbf{1})|^2]. \end{aligned} \tag{A17}$$

As in the computation of the energy, it is convenient to isolate the $\vec{G}\to 0$ contribution since it usually gives rise to nonanalyticities. A Taylor expansion for the $\mathbf{G}\to 0$ contribution leads to a final expression

$$\begin{aligned} \Pi_{\alpha\beta}(\vec{p}) &= \frac{2^{2-\gamma}\pi\Gamma(1-\gamma/2)}{A_C\Gamma(\gamma/2)}\frac{\vec{p}_\alpha\vec{p}_\beta}{|\vec{p}|^{2-\gamma}} + \frac{2^{2-\gamma}\pi\Gamma(1-\gamma/2)}{A_C\Gamma(\gamma/2)}\\ &\quad \times\frac{\vec{p}_\alpha\vec{p}_\beta}{|\vec{p}|^{2-\gamma}}\left[\frac{1}{\Gamma(1-\gamma/2)}\left(\frac{\vec{p}^2}{4\sigma}\right)^{1-\gamma/2}\varphi_{-\gamma/2}\left(\frac{\vec{p}^2}{4\sigma}\right)-1\right]\\ &\quad +\frac{\pi\sigma^{\gamma/2-1}}{A_C\Gamma(\gamma/2)}\sum_{\vec{G}}(\vec{p}+\vec{G})_\alpha(\vec{p}+\vec{G})_\beta\varphi_{-\gamma/2}\left(\frac{|\vec{p}+\vec{G}|^2}{4\sigma}\right)\\ &\quad -\frac{\pi\sigma^{\gamma/2-1}}{A_C\Gamma(\gamma/2)}\sum_{\vec{G}}\vec{G}_\alpha\vec{G}_\beta\varphi_{-\gamma/2}\left(\frac{|\vec{G}|^2}{4\sigma}\right)\\ &\quad -\frac{2\sigma^{\gamma/2+1}}{\Gamma(\gamma/2)}\sum_{\mathbf{1}\neq\mathbf{0}}\{1-\cos[\vec{p}\cdot\vec{R}(\mathbf{1})]\}\varphi_{\gamma/2}[\sigma|\vec{R}(\mathbf{1})|^2]\\ &\quad +\frac{4\sigma^{\gamma/2+2}}{\Gamma(\gamma/2)}\sum_{\mathbf{1}\neq\mathbf{0}}\{1-\cos[\vec{p}\cdot\vec{R}(\mathbf{1})]\}\\ &\quad \times\vec{R}(\mathbf{1})_\alpha\vec{R}(\mathbf{1})_\beta\varphi_{1+\gamma/2}[\sigma|\vec{R}(\mathbf{1})|^2]. \end{aligned} \tag{A18}$$

Since all the terms in the previous expression but the first one are analytical functions of the momentum, the response function at large distances goes like

$$\Pi_{\alpha\beta}(\vec{p}) = \frac{2^{2-\gamma}\pi\Gamma(1-\gamma/2)}{A_C\Gamma(\gamma/2)}\frac{\vec{p}_\alpha\vec{p}_\beta}{|\vec{p}|^{2-\gamma}} + A_{\alpha\beta\mu\nu}\vec{p}^\mu\vec{p}^\nu + B_{\alpha\beta\mu\nu\rho\zeta}\vec{p}^\mu\vec{p}^\nu\vec{p}^\rho\vec{p}^\zeta + O(\vec{p}^6).$$

(A19)

The results derived are valid for any Bravais lattice. Again, only the triangular lattice is of interest in this paper. The tensor $A_{\alpha\beta\mu\nu}$ for the triangular lattice is[65]

$$
\begin{aligned}
A_{\alpha\beta\mu\nu} = &-\frac{\delta_{\mu\nu}}{4\Gamma(\gamma/2)}\left(\frac{\pi}{A_c}\right)^{\gamma/2-1}\sum_{\mathbf{1}\neq\mathbf{0}}G_\alpha(\mathbf{1})G_\beta(\mathbf{1})\varphi_{1-\gamma/2}\left(\frac{\pi}{A_C}\vec{R}^2(\mathbf{1})\right) - \frac{\delta_{\alpha\mu}\delta_{\beta\nu}+\delta_{\alpha\nu}\delta_{\beta\mu}}{2\Gamma(\gamma/2)}\left(\frac{\pi}{A_C}\right)^{\gamma/2}\left[\frac{2}{2-\gamma}-\sum_{l\neq0}\varphi_{-\gamma/2}\left(\frac{\pi}{A_C}\vec{R}^2(\mathbf{1})\right)\right] \\
&-\frac{1}{4^\ddagger\Gamma(\gamma/2)}\left(\frac{\pi}{A_C}\right)^{\gamma/2-1}\sum_{\mathbf{1}\neq\mathbf{0}}\left[[G_\alpha(\mathbf{1})G_\mu(\mathbf{1})\delta_{\beta\nu}+G_\beta(\mathbf{1})G_\nu(\mathbf{1})\delta_{\alpha\mu}+G_\alpha(\mathbf{1})G_\nu(\mathbf{1})\delta_{\beta\mu}+G_\beta(\mathbf{1})G_\mu(\mathbf{1})\delta_{\alpha\nu}]\varphi_{1-\gamma/2}\left(\frac{\pi}{A_C}\vec{R}^2(\mathbf{1})\right)\right] \\
&+\frac{1}{8\Gamma(\gamma/2)}\left(\frac{\pi}{A_C}\right)^{\gamma/2-2}\sum_{\mathbf{1}\neq\mathbf{0}}G_\alpha(\mathbf{1})G_\beta(\mathbf{1})G_\mu(\mathbf{1})G_\nu(\mathbf{1})\varphi_{2-\gamma/2}\left(\frac{\pi}{A_C}\vec{R}^2(\mathbf{1})\right) \\
&+\frac{2}{\Gamma(\gamma/2)}\left(\frac{\pi}{A_C}\right)^{\gamma/2+2}\sum_{\mathbf{1}\neq\mathbf{0}}R_\alpha(\mathbf{1})R_\beta(\mathbf{1})R_\mu(\mathbf{1})R_\nu(\mathbf{1})\varphi_{1+\gamma/2}\left(\frac{\pi}{A_C}\vec{R}^2(\mathbf{1})\right) - \frac{\delta_{\mu\nu}}{\Gamma(\gamma/2)}\left(\frac{\pi}{A_C}\right)^{\gamma/2+1}\sum_{\mathbf{1}\neq\mathbf{0}}R_\alpha(\mathbf{1})R_\beta(\mathbf{1})\varphi_{\gamma/2}\left(\frac{\pi}{A_C}\vec{R}^2(\mathbf{1})\right).
\end{aligned}
$$

(A20)

The form of the elastic tensor can be parametrized by two coefficients $\theta(\gamma)$ and $\eta(\gamma)$,

$$A_{\alpha\beta\mu\nu} = \frac{\eta(\gamma)}{A^{\gamma/2}}[\delta_{\mu\nu}\delta_{\alpha\beta} + \rho(\gamma)(\delta_{\mu\alpha}\delta_{\nu\beta} + \delta_{\mu\beta}\delta_{\nu\alpha})],$$

(A21)

a result that can just follow from the symmetry properties of the triangular lattice.[62]

APPENDIX B: MATHEMATICAL IDENTITIES USED

In this section useful mathematical identities are listed without further remarks to make the paper as self-contained as possible and for the purpose of fixing the notation.

1. Identities present in Ewald sums

(i) The gamma identity,

$$\frac{1}{|\vec{x}|^\gamma} = \frac{1}{\Gamma\left(\frac{\gamma}{2}\right)}\int_0^\infty dt\, t^{-1+(\gamma/2)}e^{-t|\vec{x}|^2}.$$

(B1)

(ii) Misra function definition,

$$\varphi_n(z) = \int_1^\infty dt\, t^n e^{-zt}.$$

(B2)

(iii) Misra function derivatives,

$$\nabla_{\vec{x}}\varphi_n(a|\vec{x}-\vec{m}|^2) = -2a(\vec{x}-\vec{m})\varphi_{1+n}(a|\vec{x}-\vec{m}|^2),$$

(B3)

$$
\begin{aligned}
\frac{\partial^2}{\partial_\alpha\partial_\beta}\varphi_n(a|\vec{x}-\vec{m}|^2) = &-2a\delta_{\alpha\beta}\varphi_{1+n}(a|\vec{x}-\vec{m}|^2) \\
&+4a^2(\vec{x}-\vec{m})_\alpha(\vec{x}-\vec{m})_\beta\varphi_{n+2}(a|\vec{x}-\vec{m}|^2).
\end{aligned}
$$

(B4)

(iv) Poisson summation formula for Gaussian integrals,

$$\sum_l e^{i\vec{q}\cdot(\vec{x}-\vec{R}(n))}e^{-t\sigma|\vec{x}-\vec{R}(\mathbf{1})|^2} = \frac{\pi}{A_C t\sigma}\sum_{\vec{G}}e^{i(\vec{G}+\vec{q})\vec{x}}e^{-(|\vec{q}+\vec{G}|^2)/4t\sigma}.$$

(B5)

[1] J. J. Thomson, Philos. Mag. **7**, 237 (1904).

[2] E. B. Saff and A. B. J. Kuijlaars, Math. Intell. **19**, 5 (1997).

[3] D. P. Hardin and E. B. Saff, Not. Am. Math. Soc. **51**, 1186 (2005).

[4] D. P. Hardin and E. B. Saff, Adv. Math. **193**, 174 (2005).

[5] U. Albrecht and P. Leiderer, J. Low Temp. Phys. **86**, 131 (1992).

[6] P. Leiderer, Z. Phys. B: Condens. Matter **98**, 303 (1993).

[7] C. C. Grimes and G. Adams, Phys. Rev. Lett. **42**, 795 (1979).

[8] D. C. Glattli, E. Y. Andrei, and F. I. B. Williams, Phys. Rev. Lett. **60**, 420 (1998).

[9] P. Lenz and D. R. Nelson, Phys. Rev. Lett. **87**, 125703 (2001); Phys. Rev. E **67**, 031502 (2003).

[10] E. J. Davis, Aerosol Sci. Technol. **26**, 212 (1997).

[11] D. L. D. Caspar and A. Klug, Cold Spring Harb Symp. Quant Biol. **27**, 1 (1962).

[12] C. J. Marzec and L. A. Day, Biophys. J. **255**, 1 (1993).

[13] X. Yan, N. H. Olson, J. L. Van Etten, M. Bergoin, M. G. Rossmann, and T. S. Baker, Nat. Struct. Biol. **7**, 101 (2000).

[14] T. S. Baker, N. H. Olson, and S. D. Fuller, Microbiol. Mol. Biol. Rev. **63**, 862 (1999).

[15] R. Zandi, D. Reguera, R. F. Bruinsma, W. M. Gelbart, and J. Rudnick, Proc. Natl. Acad. Sci. U.S.A. **101**, 15556 (2004).

[16] J. Lidmar, L. Mirny, and D. R. Nelson, Phys. Rev. E **68**, 051910 (2003).

[17] S. Jain and D. R. Nelson, Phys. Rev. E **61**, 1599 (2000).

[18] A. Pérez-Garrido, M. J. W. Dodgson, and M. A. Moore, Phys. Rev. B **56**, 3640 (1997).

[19] A. Toomre (private communication).

[20] A. Pérez-Garrido and M. A. Moore, Phys. Rev. B **60**, 15628 (1999), and references therein.

[21] M. J. Bowick, D. R. Nelson, and A. Travesset, Phys. Rev. B **62**, 8738 (2000).

[22] A. R. Bausch, M. J. Bowick, A. Cacciuto, A. D. Dinsmore, M. F. Hsu, D. R. Nelson, M. G. Nikolaides, A. Travesset, and D. A. Weitz, Science **299**, 1716 (2003).

[23] P. Lipowsky, M. J. Bowick, J. H. Meinke, D. R. Nelson, and A. R. Bausch, Nat. Mater. **4**, 407 (2005).

[24] T. Einert, P. Lipowsky, J. Schilling, M. J. Bowick, and A. R. Bausch, Langmuir **21**, 12076 (2005).

[25] A. D. Dinsmore, MingF. Hsu, M. G. Nikolaides, Manuel Marquez, A. R. Bausch, and D. A. Weitz, Science **298**, 1006 (2002).

[26] H. W. Kroto, J. R. Heath, S. C. O'Brien, R. F. Curl, and R. E. Smalley, Nature (London) **318**, 162 (1985).

[27] M. J. W. Dodgson and M. A. Moore, Phys. Rev. B **55**, 3816 (1997).

[28] Y. Masuda, T. Itoh, and K. Koumoto, Adv. Mater. (Weinheim, Ger.) **17**, 841 (2005).

[29] B. Alberts *et al.*, *Molecular Biology of the Cell* (Garland Science, New York, 2002).

[30] T. Kohyama, D. M. Kroll, and G. Gompper, Phys. Rev. E **68**, 061905 (2003).

[31] K. Simons and W. L. C. Vaz, Annu. Rev. Biophys. Biomol. Struct. **33**, 269 (2004).

[32] J. Korlach, P. Schwille, W. W. Webb, and G. W. Feigenson, Proc. Natl. Acad. Sci. U.S.A. **96**, 8461 (1999).

[33] G. W. Feigenson and J. T. Buboltz, Biophys. J. **80**, 2775 (2001).

[34] D. Scherfeld, N. Kahya, and P. Schwille, Biophys. J. **85**, 3758 (2003).

[35] S. Schneider and G. Gompper, Europhys. Lett. **70**, 136 (2005).

[36] S. Chushak and A. Travesset, Europhys. Lett. **72**, 767 (2005).

[37] M. J. Bowick, A. Cacciuto, D. R. Nelson, and A. Travesset, Phys. Rev. Lett. **89**, 185502 (2002).

[38] E. L. Altschuler, T. J. Williams, E. R. Ratner, F. Dowla, and F. Wooten, Phys. Rev. Lett. **72**, 2671 (1994).

[39] E. L. Altschuler, T. J. Williams, E. R. Ratner, R. Tipton, R. Stong, F. Dowla, and F. Wooten, Phys. Rev. Lett. **78**, 2681 (1997).

[40] M. J. Bowick, C. Cecka, and A. A. Middleton, see Java applet at http://physics. syr. edu/condensedmatter/thomson/.

[41] T. Erber and G. M. Hockney, Adv. Chem. Phys. **98**, 495 (1997).

[42] J. R. Morris, K. M. Ho, D. M. Deaven, and N. Tit, Chem. Phys. Lett. **256**, 195 (1996).

[43] E. L. Altschuler and A. Perez-Garrido, Phys. Rev. E **71**, 047703 (2005).

[44] A. Travesset, Phys. Rev. B **68**, 115421 (2003).

[45] M. J. Bowick and A. Travesset, J. Phys. A **34**, 1535 (2001).

[46] F. David, E. Guitter, and L. Peliti, J. Phys. (France) **48**, 1085 (1987).

[47] U. B. Sleytr, M. Sára, D. Pum, and B. Schuster, Prog. Surf. Sci. **68**, 231 (2001).

[48] D. Pum, P. Messner, and U. B. Sleytr, J. Bacteriol. **173**, 6865 (1991).

[49] D. R. Nelson, in *Statistical Mechanics of Membranes and Surfaces*, 2nd ed., edited by D. Nelson, T. Piran, and S. Weinberg (World Scientific, Singapore, 2004), Chaps. 1 and 6.

[50] F. David, in *Statistical Mechanics of Membranes and Surfaces*, 2nd ed., edited by D. Nelson, T. Piran, and S. Weinberg (World Scientific, Singapore, 2004), Chap. 7.

[51] K. J. Wiese, "Polymerized membranes, a review," in *Phase Transitions and Critical Phenomena*, edited by C. Domb and J. L. Lebowitz (Academic, New York, 2001), Vol. 19, p. 253.

[52] M. J. Bowick and A. Travesset, Phys. Rep. **344**, 255 (2001).

[53] M. J. Bowick, in *Statistical Mechanics of Membranes and Surfaces*, 2nd ed., edited by D. Nelson, T. Piran, and S. Weinberg (World Scientific, Singapore, 2004), Chap. 11.

[54] D. R. Nelson and L. Peliti, J. Phys. (Paris) **48**, 1085 (1987).

[55] W. Helfrich, Z. Naturforsch. C **28**, 693 (1973).

[56] D. R. Nelson, *Defects and Geometry in Condensed Matter Physics* (Cambridge University Press, Cambridge, 2002), Chap. 6.

[57] A. Travesset, Phys. Rev. E **72**, 036110 (2005).

[58] J. De Luca, S. B. Rodrigues, and Y. Levin, Europhys. Lett. **71**, 84 (2005).

[59] S. B. Dierker, R. Pindak, and R. B. Meyer, Phys. Rev. Lett. **56**, 1819 (1986); by introducing a pressure difference across the free standing liquid crystal film, one could study the 2π disclinations and grain boundaries of this reference in a hemispherical environment [R. Pindak and C. C. Huang (private communication)].

[60] L. Bonsall and A. A. Maradudin, Phys. Rev. B **15**, 1959 (1977).

[61] D. S. Fisher, B. I. Halperin, and R. Morf, Phys. Rev. B **20**, 4692 (1979).

[62] L. Landau and E. Lifshitz, *Theory of Elasticity* (Butterworth, Heinemann, 1992), Vol. 7.

[63] We follow here the traditional conventions in the literature on the Thomson problem (Ref. 41) and define the energy with a factor of 2.

[64] There is a factor of 2 implicit in that calculation.

[65] ‡: This coefficient for $\gamma=1$ differs from (Ref. 60).